Efficient Onboard Multitask AI Architecture Based on Self-Supervised Learning

Fusion Engineering and Design 209 (2024) 114713

Contents lists available at ScienceDirect

Fusion Engineering and Design

journal homepage: www.elsevier.com/locate/fusengdes

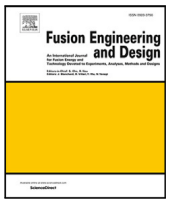

Neutron transport and activation comparison between OpenMC and FISPACT-II in ARC-class reactor

Davide Pettinari [a,*], Raffaella Testoni [a], Massimo Zucchetti [a,b], Miriam Parisi [c]

[a] Department of Energy, Politecnico di Torino, Corso Duca degli Abruzzi 24, Torino, 10129, Italy
[b] MIT Plasma Science and Fusion Center, 167 Albany St, Cambridge, MA, 02139, United States of America
[c] MAFE, Eni S.p.A., Via A. Pacinotti 4, Venezia, 30175, Italy

ARTICLE INFO

Keywords:
ARC reactor
Neutronics
Neutron damage
Activation
OpenMC
FISPACT-II
Code-to-code comparison

ABSTRACT

In a fusion reactor, high-energy neutron fluxes strike the materials causing radiation damage and triggering nuclear reactions that alter the chemical composition of the materials through transmutation. This investigation employs the Monte Carlo code OpenMC with Direct Accelerated Geometry Monte Carlo (DAGMC), a software package that allows users to perform Monte Carlo radiation transport directly on CAD models. The analysis was conducted on an Affordable Robust Compact (ARC) class reactor using a 3D CAD geometry. OpenMC supports depletion calculations allowing for the time evolution of the radioactive inventories evaluation. This study focuses on the machine's nuclear performance, analyzing tritium production, neutron fluxes, and power deposition to assess the reactor's behavior. It also explores the primary aspects of neutron irradiation on solid materials in the ARC class reactor, with particular emphasis on neutron-induced activation and displacements per atom (DPA). The neutronic results indicate that the predicted tritium breeding ratio and power density are consistent with both the reactor design specifications and the findings in existing literature, while the DPA and activation calculations reveal key areas of material degradation due to neutron irradiation. To validate the accuracy of the results, a comparison was made with corresponding results obtained using the FISPACT-II code. The agreement between the two codes serves as a benchmark for the reliability of OpenMC in predicting nuclear activation phenomena in fusion reactors.

1. Introduction

The growing need to expand global energy production capacity, alongside the urgent requirement to reduce carbon dioxide emissions, catalyzes the development and diversification of concepts for energy production. Recent evolution in this field leans towards the design of more compact reactors, moving beyond the traditional paradigms of large-scale facilities characterized by high costs and extended construction periods. This trend is made possible by the advent of High Temperature Superconductors (HTS), which enable the design of high magnetic field systems and the consequent reduction of plant size. The ARC design features the use of Rare Earth Barium Copper Oxide (REBCO) superconducting toroidal coils, modularity in construction, and the adoption of an all-liquid blanket, composed of FLiBe (lithium and beryllium fluoride), a molten salt that acts as a neutron moderator, neutron shield, coolant and tritium breeder. Given the production of fast neutrons at 14.1 MeV from the deuterium–tritium (D–T) fusion reaction, the FLiBe blanket proves to be effective in moderating neutrons, providing shielding, and removing heat, significantly contributing to the sustainability of the fusion process [1,2].

Simultaneously, the selection of materials for plasma-facing components, such as the first wall and the vacuum vessel, becomes critically relevant as they need to withstand both the high neutron flux and the corrosion induced by the molten salt. The aim of this work is to thoroughly examine the neutronic and activation issues within such a reactor to assess its feasibility. This study integrates both neutron transport and activation modeling, providing a comprehensive understanding of the reactor's operational challenges and long-term sustainability. In particular, material activation plays a crucial role, directly impacting the reactor's economy in terms of decommissioning and radioactive waste management. Therefore, it is essential that these materials exhibit low levels of activation. These analyses were performed using two distinct codes: OpenMC and FISPACT-II, which differ significantly in scope and purpose. FISPACT-II is an activation solver designed to model material activation and decay over time, providing insights into radionuclide inventories and activity [3]. OpenMC is a Monte Carlo particle transport code that simulates the interaction and transport of particles, such as neutrons, through materials [4].

* Correspondence to: DENERG, Politecnico di Torino, Italy
E-mail address: davide.pettinari@polito.it (D. Pettinari).

https://doi.org/10.1016/j.fusengdes.2024.114713
Received 3 July 2024; Received in revised form 13 October 2024; Accepted 3 November 2024
Available online 16 November 2024

Studies have shown that materials such as stainless steel and Inconel-718 can become highly activated, posing challenges for their use in reactor environments. The presence of nickel in alloys leads to the formation of long-lived radionuclides, exacerbating waste management issues [5,6]. Activation due to high-energy neutrons is particularly problematic as it can result in the production of radionuclides, including those with long half-lives.

This paper presents and investigates a 360-degree 3D CAD model of an ARC-class reactor consistent with the geometry presented in the work [1,2,7,8]. The 3D geometry allows for a more detailed representation of the spatial distribution of materials and reactor components and can improve the accuracy of neutron calculations, it should be noted that the components are still homogenized, and thus the exact 'as-built' geometry is not fully represented. This approach allows for capturing local variations in neutron flux, which can vary significantly within the reactor. This is crucial for identifying areas of high and low neutron flux intensity.

OpenMC stands out as a powerful open-source Monte Carlo simulation code developed for high fidelity neutron and photon transport simulations. Developed since 2011 by members of the Computational Reactor Physics Group at the Massachusetts Institute of Technology and Argonne National Laboratory together with a global community of developers, OpenMC supports detailed modeling of neutron interactions, which are crucial for accurate reactor analysis and safety assessments [9]. OpenMC supports transport-coupled and transport-independent depletion. The software uses transmutation reaction rates to solve a set of transmutation equations that determine the evolution of nuclide densities within a material [10]. The nuclide densities predicted at some future time are then used to determine updated reaction rates, and the process is repeated for as many timesteps as requested. OpenMC utilizes the Direct Accelerated Geometry Monte Carlo (DAGMC) toolkit to represent CAD-based geometries in a surface mesh format. DAGMC, developed by the University of Wisconsin-Madison, is an advanced toolset designed to facilitate Monte Carlo particle transport simulations directly on CAD models [11].

FISPACT-II is a software developed by the UK Atomic Energy Authority (UKAEA) for simulating neutron activation and nuclear transmutation [3,12]. This tool is employed to assess irradiation effects on materials exposed to neutron fluxes, which are commonly found in nuclear reactors and fusion devices. This code excels in predicting the generation and decay of radioactive isotopes, as well as calculating critical metrics such as residual heat, radiation doses, isotope production rates, and specific activity. These capabilities make FISPACT-II indispensable for managing spent fuel and activated materials, reactor design, and evaluating the environmental impact of nuclear technologies.

2. Methods

In this study, a comparison is conducted between OpenMC (version 0.14.0) and FISPACT-II (version 4.0) regarding the activation analysis of structural materials in an ARC-class reactor. To ensure the transparency of the comparison, both codes utilize the same nuclear data library, specifically the ENDF/B-VII.1 Evaluated Nuclear Data Library, which includes incident neutron, photoatomic, thermal scattering, and windowed multipole data. The HDF5 files required by OpenMC are created by the code development team by converting the source ENDF files to ACE files using NJOY 2016.68 [13], then using the openmc.data Python module to convert the ACE data to HDF5.

The analysis begins with OpenMC, conducting a neutronic study on a three-dimensional model of the machine. This assessment allows the evaluation of the reactor's neutron economy, power deposition in various zones, neutron fluxes and spectra, as well as displacement per atom. Data concerning neutron fluxes and spectra are subsequently used as inputs for FISPACT-II, to proceed with the activation analysis. This analysis includes the evaluation of displacement per atom, specific activity, decay heat output, and dose rate.

A second analysis is later performed with OpenMC in depletion mode, where decay heat and specific activity are determined. The results obtained from both software tools are then compared with respect to decay heat output, specific activity, and displacement per atom.

The comparison highlights significant differences in how the two codes process data: while OpenMC conducts a three-dimensional analysis directly on the provided CAD model, FISPACT-II operates with a reduced input set, including neutron spectra and fluxes, as well as the volume, weight, and chemical composition of the material, conducting a zero-dimensional (0D) analysis. This study provides a clear insight into how the two codes differ in their approach to activation analysis and the impact of these differences on the obtained results. The study has followed the process shown in Fig. 1

2.1. CAD-based geometry

The reactor model used, the same as in works [7,8] is presented in Fig. 2. The three-dimensional geometry of the reactor is developed by using the computer-aided design software SolidWorks®. The resulting model comprises eight distinct regions, collectively divided into forty-three volumes. The inner component of the device, designated for plasma generation, is modeled as a singular volume, similarly to the blanket and surrounding tank wall. Due to their minimal thickness and proximity to the neutron source, the internal areas such as the first wall, the vacuum vessel (both inner and outer sections), the neutron multiplier, and cooling channels are subdivided into eight distinct volumes each, to facilitate a detailed neutronic analysis as shown in Fig. 3.

Following the modeling phase, each volume is exported from the native SolidWorks® format (.SLDPRT) to the Standard Tessellation Language (.STL) format, which represents the geometric surface of the model using triangles. Subsequently, through the use of the Python package *stl-to-h5 m 0.2.3* [14], the STL files are converted into Direct Accelerated Geometry Monte Carlo (DAGMC) h5 m files, ready for use in neutronic simulations [15]. Since this meshing method does not imprint and merge the geometry, its integrity is verified using SolidWorks® and the DAGMC overlap checker [16] to ensure that no overlaps are present. This conversion method is chosen to ensure that the workflow developed is completely open source, with the exception of the CAD modeling software and FISPACT-II. All tools and libraries used, apart from these two, are available under open source licenses.

2.2. Transport problem definition

ARC-class reactor serves critical functions such as neutron shielding, power generation and tritium breeding, with this particular reactor designed to achieve a tritium breeding ratio (TBR) of at least 1.1. Since this machine has a fusion power of 525 MW [1], the number of neutrons produced by the D–T reactions is approximately 1.86×10^{20} n/s.

The materials used, detailed in the supplementary material of the work [7], include rarified hydrogen in the machine's interior to simulate vacuum conditions, tungsten for the first wall, Inconel-718 [17] for structural components (inner and outer vacuum vessel and tank wall), beryllium as a neutron multiplier, and FLiBe for the cooling channels and blanket. Notably, the lithium in FLiBe has been enriched to 90% lithium-6 to enhance the number of n+^{6}Li reactions, thereby increasing tritium production and improving shielding.

The neutron source is generated using the Python-based package *OpenMC-plasma-source 0.3.1* [18], which provides a collection of pre-built sources for use, specifically employing the tokamak source to create a source with spatial and temperature distributions characteristic of tokamak plasma. OpenMC sources are designed as ring sources to reduce computational costs, with each source having its own strength or probability that a neutron will spawn in this location.

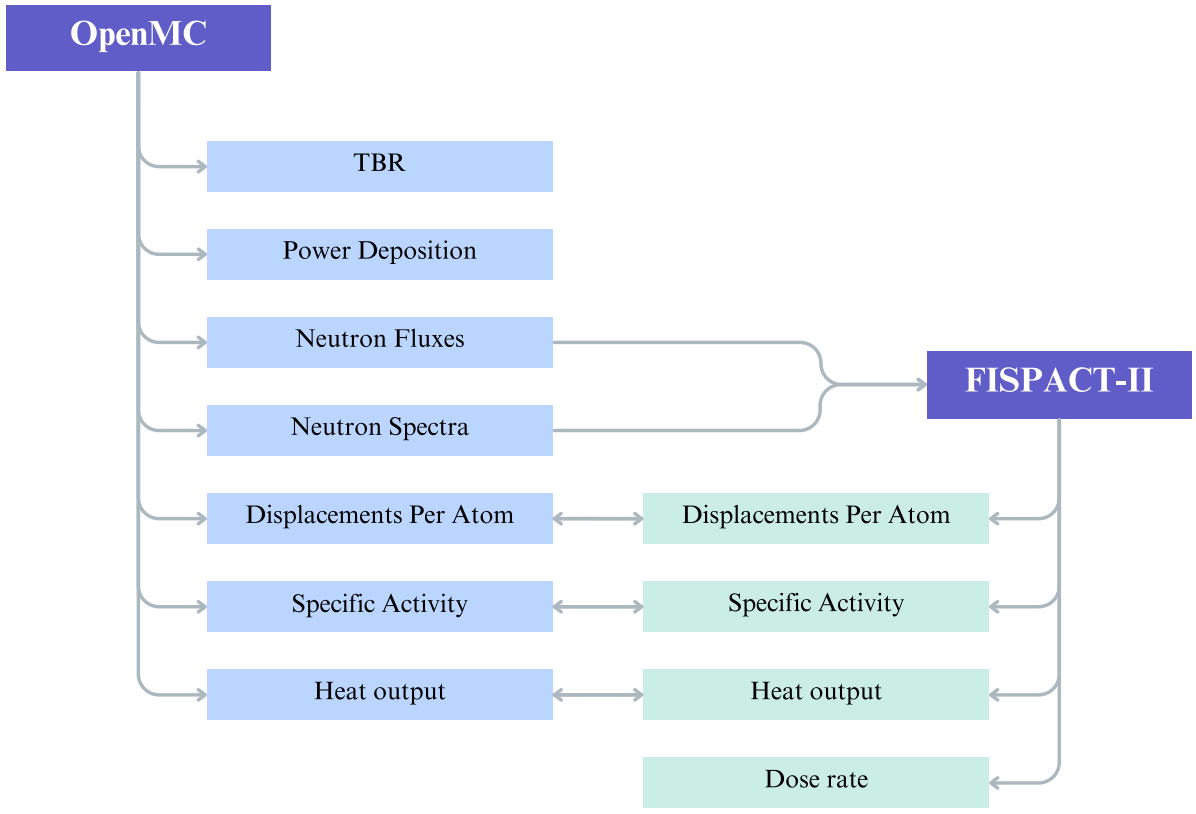

Fig. 1. Flowchart of the methodological approach. The diagram illustrates the steps followed in the work.

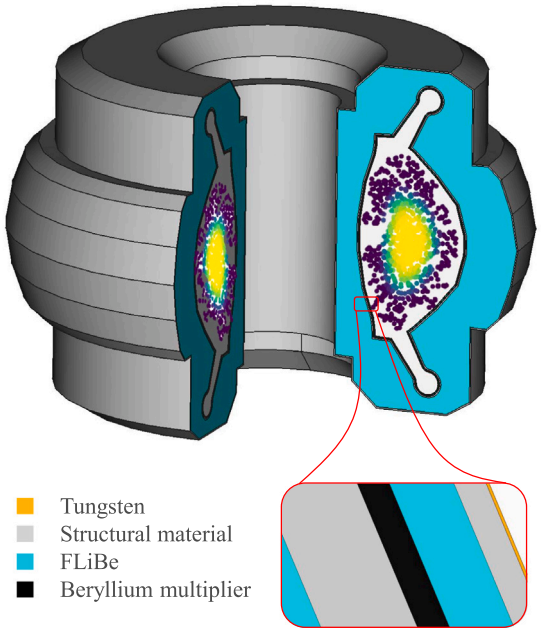

Fig. 2. Three-dimensional representation of the ARC-class reactor including the neutron source inside. There is a detailed zoom illustrating the arrangement of the various internal layers.

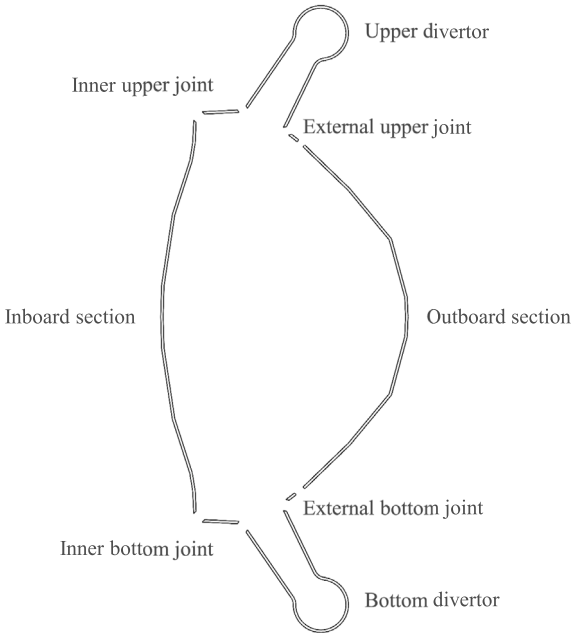

Fig. 3. Detail of the structural subdivision of the model, shown through the decomposition of the internal machine layers into 8 regions.

Neutron interactions with materials can lead to photon production through processes such as radiative capture (n, γ) and inelastic scattering. These photons can subsequently influence the surrounding environment through mechanisms like the photoelectric effect, Compton scattering, and pair production [19], which generates positrons and electrons crucial for power deposition. For this reason, both neutrons and photons were simulated in this study.

The simulation modeled power deposition, material damage, TBR, neutron flux and neutron spectra, using over 1×10^9 particles run on a high-performance computing (HPC) system. By dividing each internal layer into eight distinct regions, detailed evaluations of material

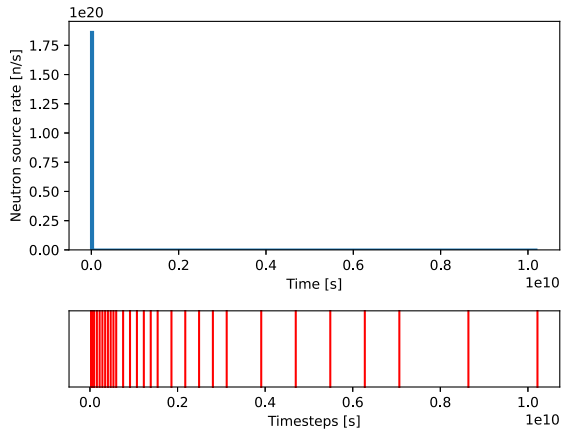

Fig. 4. Pulse schedule. The figure displays plots of source rates as a function of time, alongside a representation of the time intervals during which activation calculations are performed.

behavior under irradiation were possible, allowing precise assessments in any given zone. This approach has facilitated the identification of areas within the vacuum vessel that are more susceptible to damage and those that demonstrate greater durability, in consideration of the scheduled replacement of the component every two years [2].

2.3. Inventory and activation code definition

As for the neutron analysis, the procedure involves importing the CAD model, defining the materials and the neutron source. Three separate simulations are run, with each material depleted in turn: in the first simulation tungsten, in the second one Inconel-718 in the first structural layer and in the last one Inconel-718 in the second structural layer. The analysis is conducted on the entire layer rather than the eight sub-sections into which it is divided.

The `CoupledOperator` is employed to manage depletion, specifying in the model the decay chain file that describes the probabilities of transformation between isotopes and their half-lives. During this phase, time steps and corresponding source fractions for the irradiation program are established. The PredictorIntegrator, a fast first-order integrator, has been selected as the depletion operator for this study.

Finally, an output file will be generated, documenting the material composition at each defined time interval. The selected time intervals are consistent with those used in FISPACT-II and are illustrated in Fig. 4.

As both codes have previously been validated in analyses of smaller volumes [20,21], this study aims to evaluate the behavior of the two systems in a more significant volume.

3. Neutronics

Understanding neutron behavior in a fusion reactor is crucial for optimizing the reaction and minimizing undesired side effects, such as material damage and radioactive waste production. Neutronics studies provide essential data for assessing the safety, efficiency, and economic viability of a fusion reactor [5].

These simulations are vital for determining the spatial and energetic distribution of neutrons, which in turn influences the design of the blanket, the first wall, and other critical structures of the reactor. The assessment of neutron flux and spectrum has been particularly focused on high-risk regions. This process can aid in optimizing materials and shielding techniques to extend the reactor's operational life and reduce maintenance costs.

This section shows the results obtained from the neutronics analysis, highlighting the challenges encountered in modeling the complex phenomena associated with neutron interaction with various reactor components.

The assessment of radiation-induced damage in materials is detailed in Section 4.1, where it is juxtaposed with the findings derived from FISPACT-II.

Table 1
TBR reported in both the cooling channel and the blanket for each nuclide.

	Tritium Breeding Ratio [–]			
	^{6}Li	^{7}Li	^{9}Be	Total
Cooling channel	0.2357 ± 0.0001	0.0022 ± 0.0001	0.0006 ± 0.0001	0.2385 ± 0.0001
Blanket	0.8238 ± 0.0001	0.0071 ± 0.0001	0.0011 ± 0.0001	0.8320 ± 0.0001
Total	1.0595 ± 0.0001	0.0093 ± 0.0001	0.0017 ± 0.0001	1.0705 ± 0.0001

3.1. Tritium breeding ratio

The Tritium Breeding Ratio (TBR) quantifies the ratio between tritium atoms produced and those consumed during fusion reactions within a reactor. In the context of an ARC-class reactor, tritium is primarily generated in the cooling channel and the blanket, where neutrons initiate (n, Xt) reactions with FLiBe atoms.

To ensure a fusion reactor's self-sufficiency in tritium production, it is critical that the TBR is at least 1.0. This indicates that the reactor produces at least as much tritium as it consumes. However, aiming for a TBR slightly above one is prudent to compensate for potential losses, material absorptions, and to stockpile tritium for restarting the reactor after maintenance operations or for initiating future machines. Dynamic fuel cycle analyses have shown that low tritium combustion efficiency (TBE < 1%, ratio of tritium burn rate to tritium injection rate) requires high TBR values in the breeder region (TBR > 1.1) [22]. This study examined whether this value was achievable with the geometrical configuration and materials considered.

The choice of materials for the breeder and structural components is crucial, as materials that capture a high number of neutrons can enhance magnet protection and reduce neutron leakage. However, these materials can compromise the reactor's neutron economy by decreasing tritium production. Thus, an optimal balance is necessary [23].

The two primary tritium breeding reactions are from ^{6}Li (n, Xt) and ^{7}Li (n, Xt), respectively. Within the reactor, over 22% of the produced tritium is generated in the FLiBe cooling channel. Additionally, a small percentage of tritium, approximately 0.2%, is produced in the area of the neutron multiplier, while beryllium-9 in the breeding blanket contributes about 0.15% to the overall TBR.

Table 1 shows the TBR values.

3.2. Neutron spectra

Neutron flux [$cm^{-2}\,s^{-1}$] represents the neutron distribution within the machine. In OpenMC, a flux score on a cell returns the average distance neutrons travel through the cell. The tally is reported in units of 'neutron cm per source neutron,' which can be converted to the standard units by dividing by the cell volume and scaling by the neutron emission rate.

An increase in neutron flux corresponds to an enhanced power deposition, tritium production, material damage, and activation, as a greater number of neutrons leads to an increase in nuclear interactions. Control of neutron flux is essential for regulating reactor power, assessing safety and shielding, and analyzing the durability of the materials used.

The neutron spectrum describes the energy distribution of neutrons within the reactor, providing crucial information on the energy spread among fast, thermal, and epithermal neutrons.

The calculation of neutron flux and spectrum across eight different zones of each analyzed layer has allowed a detailed mapping of neutron behavior in various parts of the reactor. The area with the maximum flux, corresponding to the 'external partition' of each layer, and the

Table 2
Average neutron flux in the various domains. Where calculated, the maximum neutron flux recorded in the layer and the minimum are also reported.

Domain	Neutron Flux [n/cm^2/s]	Neutron Flux on Subdomain [n/cm^2/s]
First wall	3.881E+14	Outboard section: 5.866E+14 – Divertor section: 1.495E+14
Inner vacuum vessel	3.763E+14	Outboard section: 5.785E+14 – Divertor section: 1.364E+14
Cooling channel	3.493E+14	Outboard section: 5.526E+14 – Divertor section: 1.147E+14
Neutron multiplier	3.414E+14	Outboard section: 5.523E+14 – Divertor section: 1.056E+14
Outer vacuum vessel	2.857E+14	Outboard section: 4.740E+14 – Divertor section: 8.155E+13
Blanket	2.873E+13	–
Tank wall	4.935E+11	–

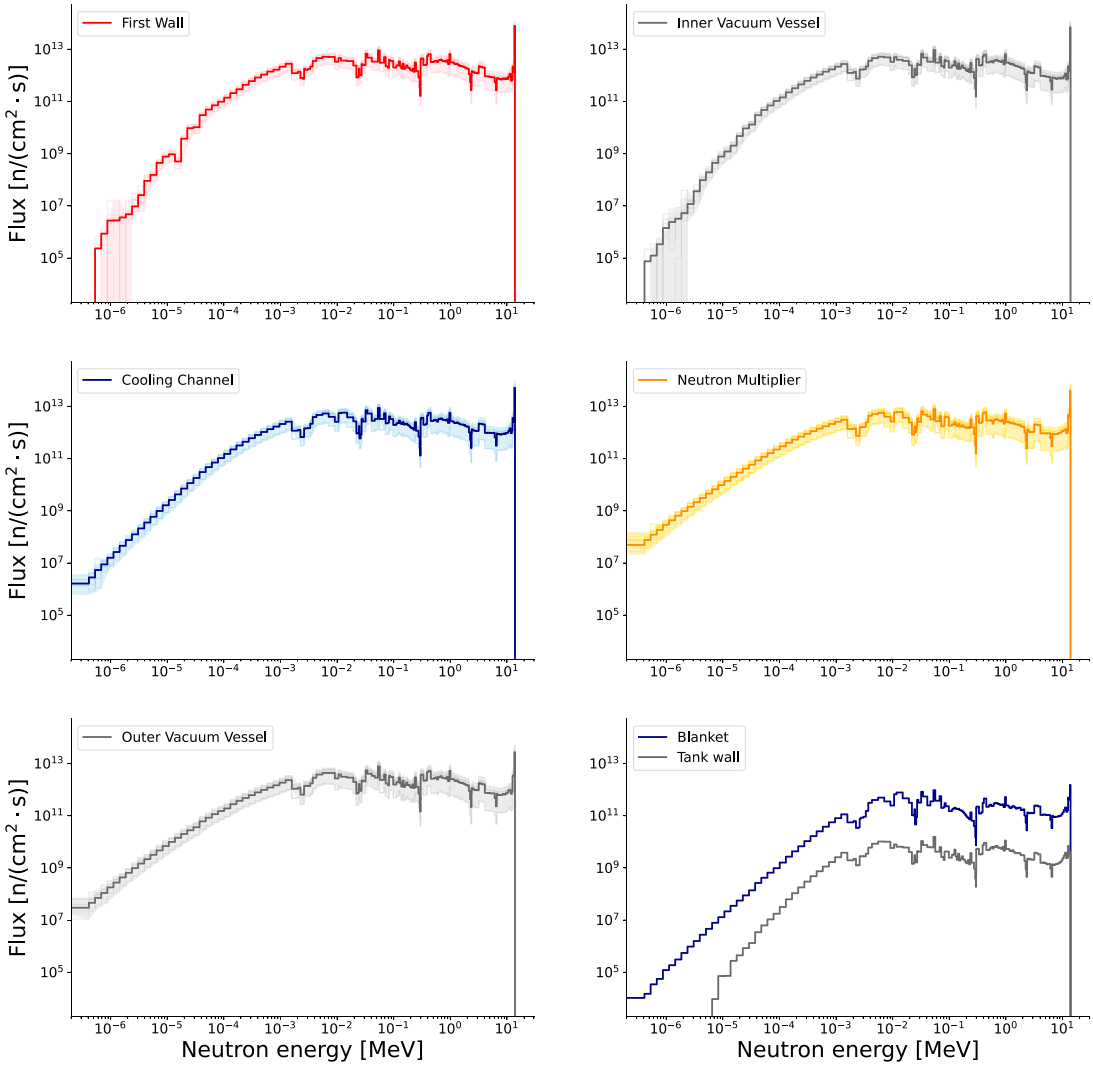

Fig. 5. Neutron flux spectrum distribution in the ARC-class reactor. The shaded areas represent the interval between the maximum and minimum neutron flux area in each layer.

area with the minimum flux, located in the divertor zone, have been identified. Notably, the area with maximum flux also coincides with the region of greatest volume in each layer.

Fig. 5 illustrates the variations in neutron spectra across each domain of the device. Specifically, each layer divided into eight parts showcases the trends in each part with a light coloration, while the average value for the entire layer is represented in a more intense color. In the blanket and tank wall layers, only average trends are presented. Table 2 details the neutron flux values.

Simulations, conducted with a particle count exceeding one billion, have achieved relative percentage errors below 1%.

3.3. Power deposition

OpenMC does not support the transport of charged particles; however, charged particles (electrons, protons, alpha particles, and heavier ions) interact with nearly every atom along their path and consistently lose energy due to atomic excitation or ionization, yet continue to advance [24].

Fig. 6 illustrates a significant impact of neutron power deposition, particularly in the cooling channel (CC) and the blanket due to the high number of reactions between neutrons and lithium-6 and lithium-7 for tritium production. Additionally, a pronounced peak in power deposition from neutrons occurs in the neutron multiplier (NM) region due to (n,2n) reactions. In the first wall (FW) and structural layers

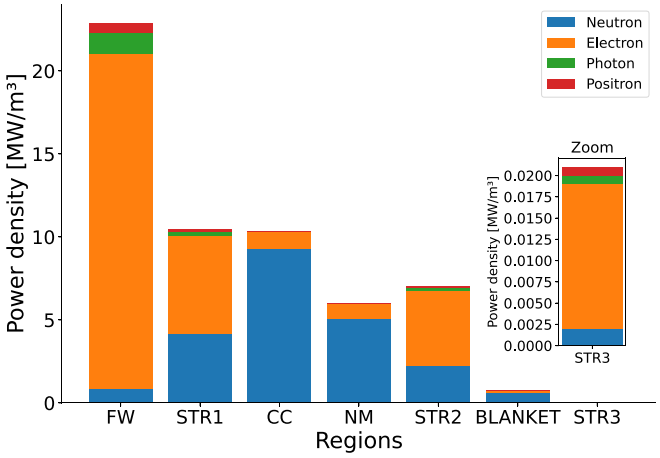

Fig. 6. Power density distribution across various regions. The contributions of neutrons, positrons, photons and electrons are clearly distinguished.

Table 3
Power deposition in each of the material layers modeled in OpenMC.

Layer	Power [MW]	Volume [m³]	Average volumetric heating [MW/m³]
Overall layer			
First wall	8.06	0.35	22.88
Inner VV	36.87	3.53	10.45
Cooling channel	73.60	7.11	10.36
Neutron multiplier	21.42	3.57	5.99
Outer VV	76.26	10.81	7.05
Blanket	258.68	350.17	0.74
Tank wall	0.28	14.00	0.02
Outboard section			
First wall	4.48	0.12	36.45
Inner VV	21.29	1.23	17.27
Cooling channel	41.48	2.49	16.68
Neutron multiplier	13.21	1.25	10.53
Outer VV	47.67	3.81	12.52
Divertor region			
Divertor First wall	0.53	0.07	7.35
Divertor Inner VV	2.08	0.73	2.87
Divertor Cooling channel	4.78	1.47	3.26
Divertor Neutron multiplier	0.96	0.74	1.29
Divertor Outer VV	3.37	2.25	1.50

(STR1, STR2, STR3), the predominant component of power deposition is from electrons. As previously mentioned, these electrons, generated from nuclear interactions of photons and neutrons, are considered to deposit their energy locally at the point of origin and are thus secondary electrons generated through nuclear interactions. The calculated and reported values are comparable with those presented in the work [25].

Total nuclear heating in units of eV per source particle were converted to MW and reported in Table 3. For neutrons, this corresponds to MT=301 produced by NJOY's HEATR module. The table presents data on power deposition across various regions within the reactor, distinguishing areas subjected to the highest and lowest neutron flux. Notably, the 'External partition' records significantly high values of power deposition, which are substantially higher than those anticipated from an averaged analysis across the entire layer.

This discrepancy highlights the localized impact of neutron flux intensities on power deposition rates and underscores the importance of detailed spatial analysis in predicting and managing thermal loads within reactor components. The observed variations in power deposition emphasize the necessity for precise monitoring and control mechanisms, particularly in regions exposed to peak neutron flux, to ensure the structural integrity and operational safety of the reactor.

4. Neutron induced activation

A detailed analysis is conducted on the structural components exposed to irradiation over a full power year. The primary focus is on neutron activation phenomena, a critical process where neutrons interact with atomic nuclei, inducing nuclear transmutations. During fusion reactions, these neutrons can activate structural materials, rendering stable atomic nuclei radioactive and transforming them into different isotopes or entirely new elements.

Particular attention is given to Inconel-718, employed in both the inner and outer vacuum vessels, and to tungsten in the first wall. These activation analyses were crucial for assessing the long-term implications of neutron exposure on structural materials, including their management according to safety and disposal criteria, as well as evaluating the materials' damage.

In accordance with recycling and disposal limits recommended by the International Commission on Radiological Protection (ICRP) [26], summarized in Table 4, it was noted that the presence of nickel in Inconel-718 significantly contributes to the increase in long-lived radionuclides. This factor poses a substantial challenge in managing the safety and recycling of materials after prolonged exposure to intense radiation. The high activation of nickel is primarily due to its isotopic composition, particularly the presence of ^{58}Ni, which undergoes a neutron capture reaction $^{58}\mathrm{Ni}(n,\gamma)^{59}\mathrm{Ni}$. Moreover, ^{59}Ni can also be produced, though less likely, via the $^{60}\mathrm{Ni}(n,2n)^{59}\mathrm{Ni}$ reaction. ^{59}Ni is a long-lived radionuclide with a half-life of approximately 76,000 years, contributing significantly to the long-term radioactivity of Inconel-718. Additionally, ^{60}Ni, another isotope of nickel, can undergo a (n,p) reaction to produce ^{60}Co, an isotope with a half-life of 5.27 years that emits strong gamma radiation. These reactions, particularly the production of ^{59}Ni and ^{60}Co, make nickel a key contributor to the activation of Inconel-718, complicating its handling and disposal in nuclear environments due to the extended period over which it remains radioactive. Nickel plays a particularly important role in the activation of Inconel-718, as it constitutes approximately 53% of the alloy. The presence of nickel isotopes, such as ^{58}Ni and ^{60}Ni, significantly contributes to the formation of long-lived radionuclides through reactions such as $^{58}\mathrm{Ni}(n,\gamma)^{59}\mathrm{Ni}$ and $^{60}\mathrm{Ni}(n,2n)^{59}\mathrm{Ni}$. In addition to nickel, several other elements in Inconel-718 contribute to its activation under neutron irradiation. The most significant among these are chromium, which makes up 19.06% of the alloy, iron at 18.15%, niobium at 5.08%, and molybdenum at 3.04%.

Chromium is responsible for several key activation reactions, such as $^{50}\mathrm{Cr}(n,\gamma)^{51}\mathrm{Cr}$, where the resulting ^{51}Cr isotope decays with a half-life of 27.7 days, emitting beta particles and gamma rays. In addition, the $^{52}\mathrm{Cr}(n,2n)^{51}\mathrm{Cr}$ reaction is notable, as well as the proton-producing reactions $^{52}\mathrm{Cr}(n,p)^{52}\mathrm{V}$ and $^{50}\mathrm{Cr}(n,np)^{49}\mathrm{V}$. Iron, another major component, undergoes activation through reactions such as $^{56}\mathrm{Fe}(n,2n)^{55}\mathrm{Fe}$, where ^{55}Fe has a half-life of approximately 2.7 years. Similarly, the $^{56}\mathrm{Fe}(n,p)^{56}\mathrm{Mn}$ reaction generates ^{56}Mn, which is highly radioactive, with an intense gamma emission and a half-life of 2.58 h. Niobium, though present in smaller quantities, plays a significant role in activation through the $^{93}\mathrm{Nb}(n,\gamma)^{94}\mathrm{Nb}$ reaction. ^{94}Nb has a long half-life of 20,300 years, making it a key contributor to long-term radioactivity in irradiated Inconel-718. Lastly, molybdenum is activated via the $^{92}\mathrm{Mo}(n,\gamma)^{93}\mathrm{Mo}$ reaction, producing ^{93}Mo, which has a half-life of around 4,000 years. This makes molybdenum another contributor to the long-term radioactive behavior of Inconel-718. Together, these reactions highlight the complexity of the activation processes in Inconel-718 and underscore the challenges in handling and recycling this material after exposure to neutron radiation.

The primary radionuclides responsible for the activation of the nickel–chromium-based superalloy are listed in Table 5. These results were obtained using FISPACT-II simulations following the irradiation of the first structural layer, providing a detailed insight into the isotopes contributing to the long-term radioactivity of the material.

Table 4
Dose rate limits for recycling purposes [27].

Industry type	Dose rate [Sv/h]	Annual limit [mSv/yr]
Nuclear Industry	1×10^{-5}	20
Other Industries	1×10^{-6}	1

Table 5
Radionuclides in Inconel-718 and their specific activity and half-life, as calculated by FISPACT-II.

Nuclide	Half-life [years]	Specific activity [Bq/kg]
^{93}Mo	4.00E+03	3.74E+08
^{59}Ni	7.60E+04	5.64E+08
^{94}Nb	2.00E+04	7.83E+08
^{91}Nb	6.80E+02	2.23E+09
^{63}Ni	1.01E+02	3.91E+10
^{93m}Nb	1.61E+01	2.84E+11
^{49}V	9.03E−01	1.93E+12
^{54}Mn	8.55E−01	2.79E+12
^{60}Co	5.27E+00	2.51E+12
^{57}Ni	4.10E−03	6.35E+12
^{60m}Co	1.99E−05	1.22E+13
^{92m}Nb	2.78E−02	1.37E+13
^{94m}Nb	1.19E−05	1.52E+13
^{52}V	7.12E−06	1.64E+13
^{56}Mn	2.95E−04	1.89E+13
^{55}Fe	2.73E+00	2.27E+13
^{51}Cr	7.58E−02	3.90E+13
^{58m}Co	1.02E−03	8.20E+13
^{57}Co	7.44E−01	1.26E+14
^{58}Co	1.94E−01	1.75E+14

4.1. Cross-code comparison results

The first parameter analyzed is the displacements per atom (DPA), widely used as an exposure unit to predict the operational lifespan of materials in radiation environments. To this end, the same calculation is made with the two softwares. In OpenMC, the process began with the production of damage energy expressed in units of eV per source particle, corresponding to MT=444 produced by the HEATR module of NJOY, and subsequently converted to DPA. The approach considers that approximately 80% of the deposited energy remains available for creating atomic displacements after 20% of it recombines to the original lattice positions.

The DPA calculation in this study follows the same methodology used by FISPACT-II, based on the Norgett–Robinson–Torrens NRT-DPA model [28], which is the international standard approach [29] for quantifying radiation damage. According to this model, the number of Frenkel pairs N_d produced in a material with displacement energy E_d (eV) for a nuclear deposited energy T_d (eV) is given by:

$$N_d = \frac{0.8T_d}{2E_d} \tag{1}$$

In the previous equation the factor 0.8 accounts for realistic atomic scattering, as opposed to the hard-core approximation. The threshold energy for atomic displacement, E_d, is material-dependent, and for this study, the same threshold values used by FISPACT-II were adopted to ensure consistency between the calculations. The specific threshold values are presented in Table 6.

The results obtained demonstrate a high degree of similarity between the two programs, confirming the reliability of the simulations conducted with both tools. This comparison not only underscores the consistency between the two methodological approaches but also how integrating their capabilities can provide a deeper and more accurate understanding of material behavior in radiation conditions.

The similarity between the results from OpenMC and FISPACT-II, shown in Table 7, consistently appears in the average values calculated across the entire material layer.

Table 6
Atomic displacement energies used to compute DPA. (E_d) is 25 eV for all other elements [12].

Element	E_d [eV]	Element	E_d [eV]
Be	31	Co	40
C	31	Ni	40
Mg	25	Cu	40
Al	27	Zr	40
Si	25	Nb	40
Ca	40	Mo	60
Ti	40	Ag	60
V	40	Ta	90
Cr	40	W	55
Mn	40	Au	30
Fe	40	Pb	25

A notable divergence is also observed in the first wall, where the DPA values calculated by OpenMC show a relative error of approximately 35% compared to FISPACT-II. This discrepancy can be attributed to several factors, the most significant being the difference in how the two codes handle DPA calculations.

FISPACT-II estimates the DPA based on the average neutron flux and average neutron spectra across the entire material layer, while OpenMC directly calculates the damage energy based on neutron interactions at a more localized level. In the case of the first wall, which is only 1 mm thick, this difference in approach becomes more pronounced. Thin layers like the first wall are highly sensitive to variations in neutron flux distribution and energy spectra, meaning that even small differences in transport modeling between the two codes can lead to greater deviations in DPA predictions.

Furthermore, by using the transport simulation code, zones subjected to higher and lower neutron fluxes were explored, enabling identification of the parts more susceptible to damage. Despite localized variations in exposure levels, all components exhibited a considerable resistance to irradiation. This resistance emphasizes the effectiveness of the materials used and the simulation techniques employed to predict structural response in high-radiation environments.

Irradiation experiments suggest that Inconel has a DPA limit of only a few tens before experiencing embrittlement and failure [30]. Therefore, the outboard section of the inner vacuum vessel is the first area that needs replacement. According to the studies [31,32], the recorded DPA values for tungsten are consistent with the material's proper functioning.

The results for specific activity and heat of decay, presented in Fig. 7, show excellent agreement between the two calculation codes. These parameters are crucial for assessing the long-term impact of irradiated materials within a reactor. Specific activity indicates the amount of radionuclides produced per unit mass of the material as a result of irradiation, while decay heat represents the thermal energy released during the radioactive decay process. These measurements are crucial for managing the safety and operational efficiency of a nuclear plant, directly influencing radioactive waste disposal strategies and the design of cooling systems.

The thick curves in the figure represent the average trend calculated over the entire analyzed layer. Nevertheless, due to the inherent differences in the codes, slight discrepancies are observed. To address these differences, additional trends were analyzed in FISPACT-II: one specific for the divertor and another for the outer partition. This analysis revealed that the trends averaged over the entire layer lie within the range defined by the areas with the highest and lowest neutron flux, i.e. the areas with the highest and lowest activation, respectively. This comparison provided an independent verification of the results, confirming that the analysis in zero dimensions (0D) provides a good approximation of that in three dimensions (3D) and demonstrating consistency in the results obtained.

The only layer for which significant differences are found is the first wall. In fact, in OpenMC, a marked reduction in the levels of specific

Table 7
Levels of neutron-induced damage in the vacuum vessel layers over a full power year, averaged across the entire poloidal cross-section with detailed assessments localized to the divertor region and the external partition.

	OpenMC			FISPACT-II
	External partition DPA/yr	Divertor DPA/yr	Average DPA/yr	Average DPA/yr
First wall	5.315	1.026	3.346	5.131
Inner vacuum vessel	18.280	3.014	11.122	10.589
Neutron multiplier	5.849	1.036	3.572	3.568
Outer vacuum vessel	12.229	1.367	6.814	7.450
Tank wall	–	–	0.009	0.010

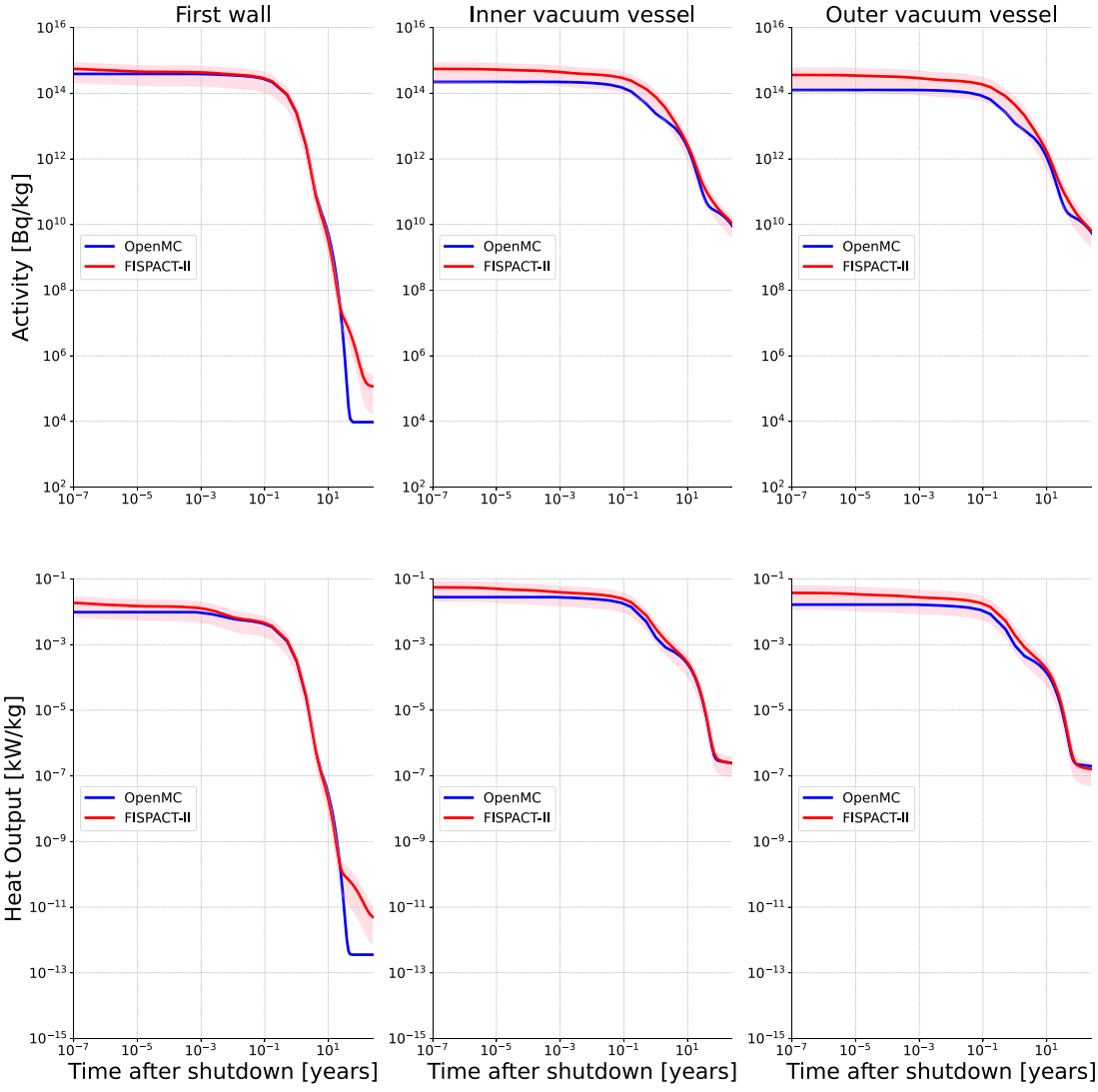

Fig. 7. Specific activity and heat output. The shaded area represents the range between the maximum and minimum value calculated in the regions of maximum and minimum neutron flux. The thick lines show the average value in the region.

activity and heat of decay is observed, unlike in FISPACT-II. Despite the fact that the exact same library was used in both codes, a discrepancy in the results is apparent.

The differences in the results are primarily due to the isotopic inventory generated as a result of the irradiation process.

Initially, the activity trends are similar between the two codes because the nuclides that contribute most significantly at this stage (such as ^{185}W, ^{181}W, and ^{186}Re) are present in comparable amounts in both FISPACT-II and OpenMC. These nuclides account for the majority of activity in the early years, and their similar abundances ensure that the overall activation shows little discrepancy between the two software packages, as shown in Table 8.

However, as time progresses, significant differences emerge, particularly from 30 years after irradiation. These discrepancies are attributed to the presence of key nuclides that influence long-term activity. Specifically, the depletion chain used by OpenMC omits important

Table 8
Primary nuclides generated in the First Wall after one year of neutron irradiation. Comparison of Activity and Atoms between FISPACT-II and OpenMC.

Nuclide	FISPACT-II		OpenMC	
	Activity [Bq]	Atoms	Activity [Bq]	Atoms
^{185}W	1.59E+18	1.49E+25	1.46E+18	1.37E+25
^{181}W	9.55E+17	1.44E+25	9.36E+17	1.41E+25
^{187}W	4.58E+17	5.67E+22	2.93E+17	3.65E+22
^{185m}W	4.50E+17	6.49E+19	4.55E+16	6.57E+18
^{183m}W	4.31E+17	3.26E+18	6.83E+13	5.12E+14
^{186}Re	2.03E+16	9.48E+21	1.56E+16	7.25E+21
^{188}Re	5.59E+15	4.93E+20	3.73E+15	3.30E+20
^{184}Re	5.15E+15	2.27E+22	4.96E+15	2.19E+22
^{182}Ta	4.66E+15	6.66E+22	4.47E+15	6.39E+22
^{179}W	4.62E+15	1.48E+19	4.73E+15	1.52E+19
^{182m}Ta	3.08E+15	1.26E+15	0.00E+00	0.00E+00
^{180}Ta	2.40E+15	1.01E+20	3.56E+15	1.51E+20
^{179}Ta	1.60E+15	1.17E+23	1.50E+15	1.25E+23
^{183}Ta	1.59E+15	1.01E+21	1.34E+15	8.51E+20
^{179m}W	9.93E+14	5.50E+17	0.00E+00	0.00E+00
^{184}Ta	9.80E+14	5.50E+17	1.34E+15	6.06E+19
^{186}Ta	5.84E+14	5.31E+17	6.05E+14	5.50E+17
^{184m}Re	5.15E+14	1.08E+22	0.00E+00	0.00E+00
^{181}Hf	3.15E+14	1.66E+21	3.55E+14	1.88E+21
^{188m}Re	2.33E+14	3.75E+17	8.30E+13	1.33E+17
^{178m}Hf	2.42E+12	1.40E+13	0.00E+00	0.00E+00
^{3}H	4.79E+11	2.69E+20	6.30E+00	3.53E+09
^{178n}Hf	2.65E+09	3.74E+18	0.00E+00	0.00E+00
^{186m}Re	3.83E+08	3.48E+21	3.02E+07	2.75E+20
^{187}Re	7.23E+06	1.43E+25	4.32E+06	8.52E+24

nuclides such as ^{182m}Ta, ^{179m}W, ^{184m}Re, ^{178m}Hf, and ^{178n}Hf. The latter two, ^{178m}Hf and ^{178n}Hf, along with ^{186m}Re, ^{186}Re, and tritium (^{3}H), are the main contributors to long-term activity.

The case of tritium is particularly notable. FISPACT-II estimates a tritium production of approximately 0.0013 g, while OpenMC calculates a significantly lower amount, around 1.77×10^{-14} g. This substantial difference in tritium production is the primary reason for the divergence in activity trends after 30 years. At this point, tritium becomes the dominant nuclide influencing the material's residual activity. However, in OpenMC, due to the much lower amount of tritium, its contribution depletes much earlier, leading to a divergence in activity compared to FISPACT-II.

The significant difference in tritium production is mainly caused by the nuclear reaction (n, t) involving the isotope ^{184}W, which constitutes approximately 30.64% of natural tungsten. This reaction, present in FISPACT-II's model, is crucial for tritium production but is not included in OpenMC's depletion chain.

In general, when using equivalent nuclear data, the predictions from OpenMC and FISPACT-II are expected to be very similar. However, there are a few subtle differences between the two codes [20]. For instance, FISPACT-II employs an approximate gamma spectrum when discrete lines are unavailable in the underlying ENDF evaluation, whereas OpenMC attempts to utilize a continuous spectrum from the ENDF evaluation, if available.

Another key difference lies in how the codes handle neutron fluxes. FISPACT-II typically requires multigroup fluxes as input and must make assumptions about the flux distribution within each group to calculate reaction rates. In contrast, OpenMC can generate the exact microscopic cross sections used for calculating reaction rates, thus offering a more precise approach in this regard.

4.2. Contact dose rate

The dose rate represents the dose of ionizing radiation delivered per unit time. This analysis aims to examine the temporal trend of the dose rate to determine compliance with the recycling limits for radioactive waste resulting from fusion, as presented in [5]. The contact dose rate plays a crucial role in defining the requirements for remote handling during recycling operations and cooling needs during the interim storage period.

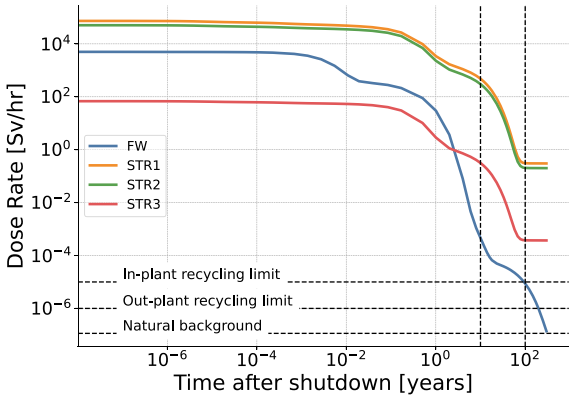

Fig. 8. Dose rate: comparison between Inconel-718 present in three different reactor zones and first wall tungsten. Results obtained using FISPACT-II.

Fig. 8 illustrates the results related to the contact dose rate. Unlike tungsten, which shows a reduction in dose rate to levels considered safe for disposal in the nuclear industry, Inconel-718 maintains excessively high values even one hundred years after radiation exposure. This persistence is also observed in areas characterized by reduced neutron flux, such as in the tank wall (STR3). This phenomenon is primarily attributable to the presence of isotopes such as ^{94}Nb, ^{59}Ni, ^{99}Tc, ^{93}Mo, and ^{99}Mo.

In the case of tungsten, the dose rate remains high before 100 years mainly due to the presence of ^{178n}Hf and ^{178m}Hf.

The initial contact dose rate of Inconel-718 is predominantly influenced by a few key isotopes, with the majority of the contribution coming from ^{58}Co, accounting for 75.4% of the total dose rate. This is followed by ^{56}Mn, contributing 8.3%, and ^{52}V with 5.95%. These nuclides, characterized by high activity and short half-lives, generate significant radiation levels immediately after irradiation.

Other isotopes, such as ^{57}Co and ^{92m}Nb, while present in lower concentrations compared to the primary contributors, add approximately 0.57% and 0.24% to the overall dose rate, respectively. Additionally, isotopes with relatively lower activity, such as ^{54}Mn, ^{24}Na, and ^{57}Ni, contribute cumulatively, though their impact remains limited compared to the dominant nuclides.

It is important to note that while short-lived nuclides like ^{58}Co dominate the initial phase, isotopes with longer half-lives (such as ^{60}Co) become more significant over time as the short-lived nuclides decay. These long-lived isotopes provide a sustained level of radiation, contributing to the long-term contact dose rate.

After more than 100 years post-irradiation, the radionuclide profile shifts, with long-lived isotopes becoming the primary contributors to the dose rate. ^{94}Nb is particularly significant at this stage, accounting for nearly the entirety of the long-term dose rate (over 99.00%), highlighting its crucial role in the later stages of decay and its impact on prolonged radiation levels.

Although this nickel-chromium superalloy is often chosen as a structural material due to its excellent thermomechanical properties at high temperatures, making it the preferred choice for structural components in fusion reactors, activation analysis reveals that it does not meet the previously mentioned low-activation criteria.

5. Conclusions

The independent validation of OpenMC and FISPACT-II, is useful for precise and comprehensive modeling of the nuclear processes taking place in an ARC-class reactor. Neutron transport was combined with

an analytical activation analysis, which allowed a detailed evaluation of nuclear reactions and their effects on the structure.

The comparison between three-dimensional and zero-dimensional analyses revealed a strong correlation in the results. While 3D simulations provide a more detailed spatial resolution, 0D models, when supplemented with accurate spectral data from 3D simulations, have proven effective for estimating many critical parameters. This approach suggests that, in certain scenarios, 0D models can serve as a complementary tool for preliminary analysis, offering time and resource efficiency without significantly compromising accuracy, as long as they are supported by detailed spectral data. However, it is important to note that FISPACT-II includes several advanced features not yet replicated in OpenMC, such as pathway analysis. Additionally, FISPACT-II's decay chains are more comprehensive than those available in OpenMC, which, as highlighted, do not include some key nuclides and reactions. Depending on specific research needs, OpenMC may or may not be a suitable alternative to FISPACT-II for comprehensive activation analysis.

Neutron irradiation damage analysis (DPA) showed that the structural materials examined do not suffer embrittlement or premature failure. This result is particularly significant for the safety and longevity of nuclear components, since embrittlement can lead to catastrophic failure. The data indicate that the materials used can maintain structural integrity. Using a 0D model, an average value was obtained that differs significantly from the maximum value. Some sections are far above the mean value, while others are far below. Therefore, for the analysis of DPA, it is more appropriate to use 3D models, which can better capture spatial variations and provide a more accurate representation of the damage distribution. Since there are areas within the reactor subjected to much higher neutron fluxes compared to others, with a view to replacing the vacuum vessel every two years, consideration could be given to not replacing the entire structure, but only the most damaged areas. This strategy would optimize costs and reduce reactor downtime by concentrating maintenance work on the most critical areas.

The study confirms that Inconel-718 is not a suitable material for use as a structural material, as it generates a high inventory of radioactive materials due to the presence of Nickel, Molybdenum and Niobium, which are high activation elements. Although very durable and suitable for high temperatures, it tends to produce a high level of nuclear activation, creating a more complex radioactive waste management. This phenomenon highlights the need to balance mechanical properties with radiological implications when choosing materials for nuclear applications. Consequently, in-depth studies on material activation are essential not only for operational purposes but also for decommissioning and radioactive waste management. Waste management and decontamination therefore become crucial aspects to consider in component design.

The overall analysis emphasizes the critical need to explore and develop new structural materials that can meet the unique challenges of nuclear fusion. The extreme conditions of temperature, radiation, stress and corrosion present in an ARC-lass reactor require materials with exceptional properties, not only in terms of mechanical strength, but also stability under neutron bombardment and low radioactive activation. Innovation in materials is crucial for the advancement of technology.

CRediT authorship contribution statement

Davide Pettinari: Writing – review & editing, Writing – original draft, Visualization, Validation, Software, Methodology, Investigation, Formal analysis, Data curation, Conceptualization. **Raffaella Testoni:** Writing – review & editing, Supervision, Project administration. **Massimo Zucchetti:** Supervision, Project administration. **Miriam Parisi:** Supervision, Project administration.

Declaration of competing interest

The authors declare that they have no known competing financial interests or personal relationships that could have appeared to influence the work reported in this paper.

Acknowledgments

The work of Davide Pettinari is part of the project PNRR-NGEU which has received funding from the MUR – DM 352/2022 and his PhD scholarship is co-funded by Eni S.p.A.. Support from CINECA for high-performance computing is also acknowledged.

Data availability

The data supporting the findings of this work are available from the corresponding authors upon reasonable request.

References

[1] B. Sorbom, J. Ball, T. Palmer, F. Mangiarotti, J. Sierchio, P. Bonoli, C. Kasten, D. Sutherland, H. Barnard, C. Haakonsen, et al., ARC: A compact, high-field, fusion nuclear science facility and demonstration power plant with demountable magnets, Fusion Eng. Des. 100 (2015) 378–405.

[2] A. Kuang, N. Cao, A.J. Creely, C.A. Dennett, J. Hecla, B. LaBombard, R.A. Tinguely, E.A. Tolman, H. Hoffman, M. Major, et al., Conceptual design study for heat exhaust management in the ARC fusion pilot plant, Fusion Eng. Des. 137 (2018) 221–242.

[3] J.-C. Sublet, J. Eastwood, J. Morgan, M. Gilbert, M. Fleming, W. Arter, FISPACT-II: an advanced simulation system for activation, transmutation and material modelling, Nucl. Data Sheets 139 (2017) 77–137.

[4] P.K. Romano, B. Forget, The OpenMC monte carlo particle transport code, Ann. Nucl. Energy 51 (2013) 274–281.

[5] S. Segantin, R. Testoni, M. Zucchetti, ARC reactor–neutron irradiation analysis, Fusion Eng. Des. 159 (2020) 111792.

[6] B. Bocci, Z. Hartwig, S. Segantin, R. Testoni, D. Whyte, M. Zucchetti, ARC reactor materials: Activation analysis and optimization, Fusion Eng. Des. 154 (2020) 111539.

[7] F. Ledda, D. Pettinari, G. Ferrero, Z. Hartwig, F. Laviano, S. Meschini, S. Sparacio, R. Testoni, D. Torsello, A. Trotta, et al., 3D neutronic analysis on compact fusion reactors: PHITS-OpenMC cross-comparison, Fusion Eng. Des. 202 (2024) 114323.

[8] F. Ledda, D. Torsello, D. Pettinari, S. Sparacio, Z. Hartwig, M. Zucchetti, F. Laviano, 3D neutronic and secondary particles analysis on $YBa_2Cu_3O_{7-\delta}$ tapes for compact fusion reactors, IEEE Trans. Appl. Supercond. (2024).

[9] P.K. Romano, N.E. Horelik, B.R. Herman, A.G. Nelson, B. Forget, K. Smith, OpenMC: A state-of-the-art Monte Carlo code for research and development, Ann. Nucl. Energy 82 (2015) 90–97.

[10] P.K. Romano, C.J. Josey, A.E. Johnson, J. Liang, Depletion capabilities in the OpenMC Monte Carlo particle transport code, Ann. Nucl. Energy 152 (2021) 107989.

[11] T.J. Tautges, P.P. Wilson, J.A. Kraftcheck, B.M. Smith, D.L. Henderson, Acceleration techniques for direct use of CAD-based geometries in Monte Carlo radiation transport, 2009.

[12] M. Fleming, T. Stainer, M. Gilbert, et al., The FISPACT-II user manual, Report UKAEA, 2018.

[13] R. Macfarlane, D.W. Muir, R. Boicourt, A.C. Kahler, III, J.L. Conlin, The NJOY Nuclear Data Processing System, Version 2016, Technical Reprt, Los Alamos National Lab.(LANL), Los Alamos, NM (United States), 2017.

[14] J. Shimwell, P. Shriwise, Stl-to-5m: Convert non overlapping STL files into a DAGMC h5m file complete with material tags and ready for use in neutronics simulations, URL https://github.com/fusion-energy/stl_to_h5m.

[15] P.C. Shriwise, X. Zhang, A. Davis, DAG-OpenMC: CAD-Based Geometry in OpenMC Patrick C. Shriwise1, Xiaokang Zhang2, Andrew Davis3 1Argonne National Laboratory 9700 Cass Ave. Argonne, IL, pshriwise@ anl. gov 2Institute of Plasma Physics, Chinese Academy of Sciences, Hefei 230031, China.

[16] B. Mouginot, A. Davis, P. Shriwise, L. Jacobson, P. Wilson, M. Harb, K. Dunn, K. Kiesling, J. Shimwell, Z. Welch, N. Granda, J. Cary, M. Nyberg, X. Zhang, V. Mahadevan, h. brooks, P. Romano, E. Biondo, C. D'Angelo, N. Schlömer, M. Renken, I. Grindeanu, E. Xu, E. Relson, C. Perry, DAGMC - direct accelerated geometry Monte Carlo toolkit, 2021, URL https://github.com/svalinn/DAGMC.

[17] A. Thomas, M. El-Wahabi, J. Cabrera, J. Prado, High temperature deformation of inconel 718, J. Mater. Process. Technol. 177 (1–3) (2006) 469–472.

[18] R. Delaporte-Mathurin, J. Shimwell, L. Pattinson, A.I. Pranto, M. Faisal, OpenMC plasma source, 2023, URL https://github.com/fusion-energy/openmc-plasma-source.

[19] K.S. Krane, Introductory Nuclear Physics, John Wiley & Sons, 1991.
[20] E.E. Peterson, P.K. Romano, P.C. Shriwise, P.A. Myers, Development and validation of fully open-source R2S shutdown dose rate capabilities in OpenMC, Nucl. Fusion 64 (5) (2024) 056011.
[21] T. Eade, B. Colling, J. Naish, L. Packer, A. Valentine, Shutdown dose rate benchmarking using modern particle transport codes, Nucl. Fusion 60 (5) (2020) 056024.
[22] S. Meschini, S.E. Ferry, R. Delaporte-Mathurin, D.G. Whyte, Modeling and analysis of the tritium fuel cycle for ARC-and STEP-class DT fusion power plants, Nucl. Fusion 63 (12) (2023) 126005.
[23] S. Segantin, R. Testoni, Z. Hartwig, D. Whyte, M. Zucchetti, Optimization of tritium breeding ratio in ARC reactor, Fusion Eng. Des. 154 (2020) 111531.
[24] N.J. Carron, An Introduction to the Passage of Energetic Particles Through Matter, Taylor & Francis, 2006.
[25] J.W. Bae, E. Peterson, J. Shimwell, ARC reactor neutronics multi-code validation*, Nucl. Fusion 62 (6) (2022) 066016.
[26] I. publication 103, The 2007 recommendations of the international commission on radiological protection, Ann. ICRP 37 (2–4) (2007) 1–332.
[27] L. Di Pace, L. El Guebaly, B. Kolbasov, V. Massaut, M. Zucchetti, et al., Radioactive waste management of fusion power plants, in: Radioactive Waste, InTech, 2012, pp. 303–328.
[28] M. Norgett, M. Robinson, I.M. Torrens, A proposed method of calculating displacement dose rates, Nucl. Eng. Des. 33 (1) (1975) 50–54.
[29] A. Standard, et al., Standard Practice for Characterising Neutron Exposure in Iron and Low Alloy Steels in Terms of Displacements Per Atom (Dpa), ASTM International, 1994.
[30] D. Michel, H. Smith, Effect of neutron irradiation on fatigue and creep-fatigue crack propagation in alloy 718 at 427°C, J. Nucl. Mater. 122 (1–3) (1984) 153–158.
[31] S. Das, Recent advances in characterising irradiation damage in tungsten for fusion power, SN Appl. Sci. 1 (12) (2019) 1614.
[32] B. Khripunov, V. Koidan, A. Ryazanov, V. Gureev, S. Kornienko, S. Latushkin, A. Rupyshev, E. Semenov, V. Kulikauskas, V. Zatekin, Study of tungsten as a plasma-facing material for a fusion reactor, Physics Procedia 71 (2015) 63–67.